Proton-Conducting Properties and Microstructure of Hydrated Tin Dioxide and Hydrated Zirconia

Shinji Hara,* Sanae Takano, and Masaru Miyayama

Institute of Industrial Science, the University of Tokyo, 4-6-1 Komaba, Meguro-ku, Tokyo, 153-8505, Japan

Received: October 9, 2003; In Final Form: February 26, 2004

The microstructure (specific surface area and pore size distribution), amount of hydrated water, and proton conductivity were examined for hydrated tin dioxide ($SnO_2 \cdot nH_2O$) and hydrated zirconia ($ZrO_2 \cdot nH_2O$), and their relationships were investigated. Both hydrates had many micropores with a pore radius below 1 nm. The average pore size of $SnO_2 \cdot nH_2O$ was smaller than that of $ZrO_2 \cdot nH_2O$. The amount of hydrated water n was 0.7−1.2 for $SnO_2 \cdot nH_2O$ and 1.0−1.7 for $ZrO_2 \cdot nH_2O$ under a relative humidity (RH) of ∼0 to 95% at 150 °C. Proton conductivity was approximately 10^{-2} S cm^{-1} under 95% RH at 150 °C for both hydrates. The conductivity decreased with decreasing RH, but $SnO_2 \cdot nH_2O$ maintained a higher conductivity than that of $ZrO_2 \cdot nH_2O$ under low RH. The high conductivity of $SnO_2 \cdot nH_2O$ at high RH despite low hydrated water content was assumed to be due to the high electronegativity of Sn and resulting high concentration of dissociated protons. The hydrated water in the small micropores of $SnO_2 \cdot nH_2O$ will be maintained even under low humidity (due to the high adsorption energy in the small micropore), and this was considered to result in the small dependence of conductivity on RH for $SnO_2 \cdot nH_2O$.

Introduction

Recently, proton conductors have been receiving increasing attention because they play very important roles in various fields, particularly as the electrolyte of fuel cells (FCs).[1−6] In FCs, the polymer electrolyte fuel cells (PEFCs) particularly have been pegged as promising power sources. PEFCs have a relatively low working temperature, and their size is easily customized, thus PEFCs meet the requirements for a wide range of applications: e.g., motors of fuel cell electric vehicles (FCEV) and home electric generators.[7,8] As the electrolyte for FCs, a polyperfluorosulfonic acid (PFSA) is generally utilized.

However, many PFSAs (e.g., Nafion, DuPont) have heat-resistance limitations, so that the working temperature of PEFCs is limited to below 100 °C.[8] If PEFCs are operated at intermediate temperatures (100−300 °C), severe poisoning of platinum-based catalyst in the electrodes by carbon monoxide included in re-formed fuel gas can be suppressed; as a result, low-purity hydrogen gas can be applied as the fuel. Also, cooling efficiency significantly improves because the temperature difference between the external air and the system of FC increases, and the reaction efficiency on electrodes and the thermal efficiency of fuel-reforming system can be enhanced.

In this manner, alternative materials that have heat resistance and a high proton conductivity are now strongly required. Furthermore, a transition from PFSA to new inexpensive materials will solve the most serious problem of the high cost of PEFCs, which is attributable to the use of expensive PFSA and platinum in electrodes. There are numerous studies on electrolytes for FCs;[9−15] however, only a few studies have been reported on practically useful electrolytes working at intermediate temperatures. Inorganic materials generally have much higher thermal stability than organic materials. It has been reported that hydrated tin dioxide ($SnO_2 \cdot nH_2O$)[16−19] and hydrated zirconia ($ZrO_2 \cdot nH_2O$)[20−28] show relatively high proton conductivities at low temperatures below 80 °C. We have confirmed their high proton conductivities under high relative humidity (RH: $= P_{H_2O}/P^\circ_{H_2O}$, $P^\circ_{H_2O}$: saturated water vapor pressure) at intermediate temperatures and found a weak dependence of conductivity on RH in $SnO_2 \cdot nH_2O$.[29,30] However, the amount and state of hydrated water and their effects on conductivity are not fully understood. In the present study, the microstructure and the amount of hydrated water were examined for $SnO_2 \cdot nH_2O$ and $ZrO_2 \cdot nH_2O$, and the relationship between the results and proton conducting properties were discussed by comparing these two hydrates.

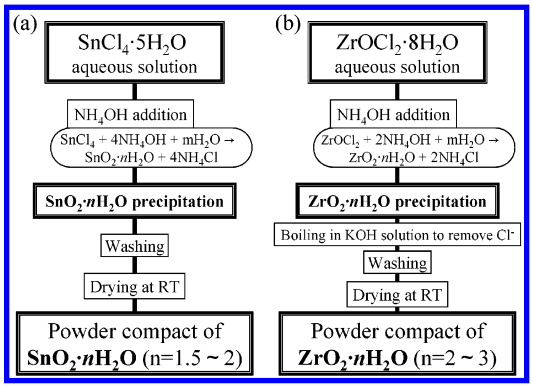

Figure 1. Synthesis of (a) $SnO_2 \cdot nH_2O$ and (b) $ZrO_2 \cdot nH_2O$.

Experimental Section

The methods of synthesizing $SnO_2 \cdot nH_2O$ and $ZrO_2 \cdot nH_2O$ are shown in Figure 1a,b, respectively. $SnO_2 \cdot nH_2O$ was prepared by adding 25% ammonia solution (NH_4OH) into tin(IV) chloride ($SnCl_4 \cdot 5H_2O$) solution, following the method described by Giesekke et al.[17] The obtained white precipitate was washed with distilled water using a centrifuge until chloride ions were no longer detected by silver nitrate ($AgNO_3$), and then dried at room temperature for 100 h. $ZrO_2 \cdot nH_2O$ was prepared by a method similar to that reported by Clearfield.[21] NH_4OH was added dropwise into zirconium oxychloride ($ZrOCl_2 \cdot 8H_2O$)

* Tel: +81 3 5452 6464. Fax: +81 3 5452 6341. E-mail: shara@iis.u-tokyo.ac.jp.

10.1021/jp0370369 CCC: $27.50
Published on Web 04/08/2004

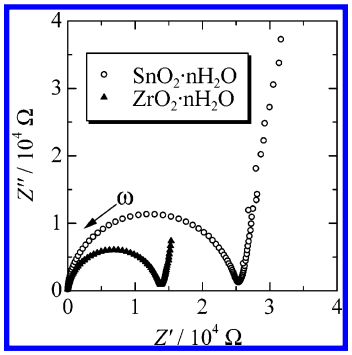

Figure 2. ac impedance profiles of $SnO_2 \cdot nH_2O$ and $ZrO_2 \cdot nH_2O$ at 18 °C in air.

solution. The obtained white precipitate was boiled in 20% potassium hydroxide (KOH) solution to remove excess chloride ions, washed in the same manner as $SnO_2 \cdot nH_2O$, and dried at room temperature for 100 h.

X-ray diffraction (XRD) profiles of these hydrates were measured with a powder diffractometer (Rint 2100, Rigaku Co.) using Cu Kα radiation under 40 kV and 20 mA at room temperature. Thermogravimetric analysis (TG) of these hydrates was conducted using a TG analysis system (Thermo Plus TG 8120, Rigaku Co.) in dry air with the heating rate of 5 °C/min at temperatures up to 500 °C. Weight changes under various water vapor pressures were recorded and the quantity of hydrated water was estimated with pressure-resistive TG apparatus (Bel Japan Inc.). The measurements were conducted after the weight changes became stable.

Adsorption measurements of nitrogen were examined at 77 K using a high-precision automatic gas adsorber (BELSORP 36, Bel Japan Inc.), and pore distributions of those hydrates were calculated by the "micropore method (MP method)"[31,32] and "Dollimore-Heal method (DH method)"[33] for the ranges of pore radii under and over 1 nm, respectively. Pretreatment of samples was conducted in vacuo for 24 h at 15 and 150 °C.

Transmission electron microscopy (TEM) images were obtained on H-9000UHR (Hitachi Co.) operating at 300 kV. Samples for observation were prepared by the powder-dispersion method.

Powders of both hydrates were pressed uniaxially into pellets of 4 mm diameter and 1−3 mm thickness at 140 MPa. Gold electrodes were sputtered onto the pellets. Conductivities of these hydrates were determined by the ac impedance method in the frequency range 5 Hz to 13 MHz with an applied voltage of 0.1 V at 20−150 °C for the samples placed in a stainless vessel. Water vapor pressure P_{H_2O} was controlled at 0.0−0.5 MPa by regulating a leak valve placed on the vessel and adjusting the temperature. Measurements were conducted after holding the sample for about 1 h at each temperature and P_{H_2O}.

Results and Discussion

Proton-Conductive Properties of $SnO_2 \cdot nH_2O$ and $ZrO_2 \cdot nH_2O$. The complex-plane impedance diagrams of $SnO_2 \cdot nH_2O$ and $ZrO_2 \cdot nH_2O$ at 18 °C in air are shown in Figure 2. In both diagrams, a part of large polarization can be observed at low frequencies (roughly below 1000 Hz), and it is assumed that Au electrodes functioned as the blocking electrode against ionic carriers. Electron conductivity was not confirmed by dc measurements. From these diagrams, proton conductivity was calculated from the resistance at the low-frequency end of the semicircle.

The temperature dependences of the conductivities of $SnO_2 \cdot nH_2O$ and $ZrO_2 \cdot nH_2O$ in air and under saturated water vapor pressure are shown in Figure 3. The conductivity of both hydrates under saturated water vapor pressure increased with increasing temperature. The highest conductivity, observed at 150 °C under $P_{H_2O} = 0.49$MPa (saturated water vapor pressure), were 2.3×10^{-2} S cm^{-1} for $SnO_2 \cdot nH_2O$ and 1.4×10^{-2} S cm^{-1} for $ZrO_2 \cdot nH_2O$. The conductivity of $ZrO_2 \cdot nH_2O$ in air started to decrease at 40 °C with increasing temperature, whereas that of $SnO_2 \cdot nH_2O$ continued to increase up to 60 °C.

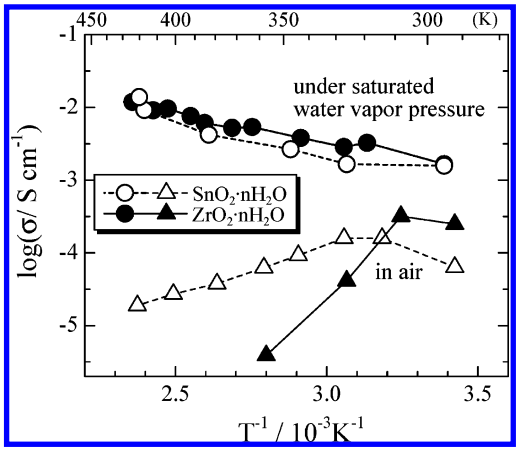

Figure 3. Temperature dependence of the conductivity for $SnO_2 \cdot nH_2O$ and $ZrO_2 \cdot nH_2O$.

The activation energies of proton conduction, estimated from the slopes of conductivity under saturated water vapor pressure, were 32 and 24 kJ mol^{-1} for $SnO_2 \cdot nH_2O$ and $ZrO_2 \cdot nH_2O$, respectively. On the basis of these values, the proton conductive mechanism of these hydrates is assumed to be the surface liquidlike water mechanism.[34] It is, therefore, thought that the same mechanism holds also in the intermediate temperature range up to 150 °C under a sufficiently high water vapor pressure.

Parts a and b of Figure 4 show the RH dependence of conductivity at 150 °C measured with decreasing RH for $SnO_2 \cdot nH_2O$ and $ZrO_2 \cdot nH_2O$, respectively. A reduction in conductivity with decreasing RH was observed for both hydrates; however, the decrease for $SnO_2 \cdot nH_2O$ was smaller than that for $ZrO_2 \cdot nH_2O$. As shown in Figure 4a, the conductivity of $SnO_2 \cdot nH_2O$ remained unchanged after repeated drying (at 150 °C, RH = 20%). On the other hand, that of $ZrO_2 \cdot nH_2O$ at low RH dropped irreversibly, as shown in Figure 4b. This result indicates that the dry-resistance property of $SnO_2 \cdot nH_2O$ is superior to that of $ZrO_2 \cdot nH_2O$. Considering the practical operation of FCs, it is preferable that electrolytes of FCs have high and stable proton conductivity even under low water vapor pressures. At this point, $SnO_2 \cdot nH_2O$ is more suitable for practical use than $ZrO_2 \cdot nH_2O$ as the electrolyte of FCs.

Microstructure of Hydrates. The powder XRD patterns for $SnO_2 \cdot nH_2O$ and $ZrO_2 \cdot nH_2O$ are shown in Figure 5a,b, respectively. Broad peaks of as-prepared samples reveal an amorphous-like state of hydrates, and the peaks sharpened with an increase in heating temperature as a result of crystallization. However, after heating, the angle of peak positions did not change and corresponded with those of the samples' oxides (SnO_2 and tetragonal ZrO_2). It can, therefore, be inferred that these hydrates consist of small particles of oxides surrounded by surface hydroxyl groups. Grain size was estimated to be about 3.0 nm, using the Scherrer equation, for both as-prepared hydrates.

Nitrogen adsorption analyses were conducted to elucidate surface conditions including the state of hydrated water for both hydrates. Nitrogen adsorption and desorption isotherms at 77 K for $SnO_2 \cdot nH_2O$ and $ZrO_2 \cdot nH_2O$ are shown in Figure 6a,b,

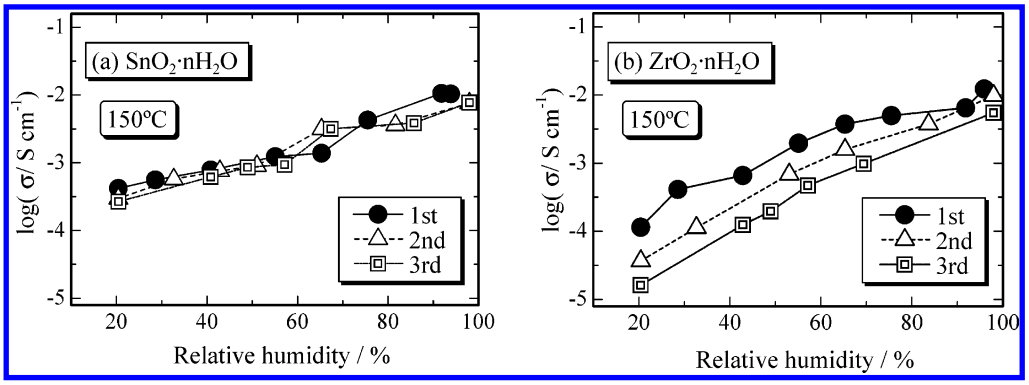

Figure 4. Relative humidity dependence of conductivity at 150 °C for (a) $SnO_2 \cdot nH_2O$ and (b) $ZrO_2 \cdot nH_2O$ upon repeated drying at 150 °C, measured with decreasing water vapor pressure.

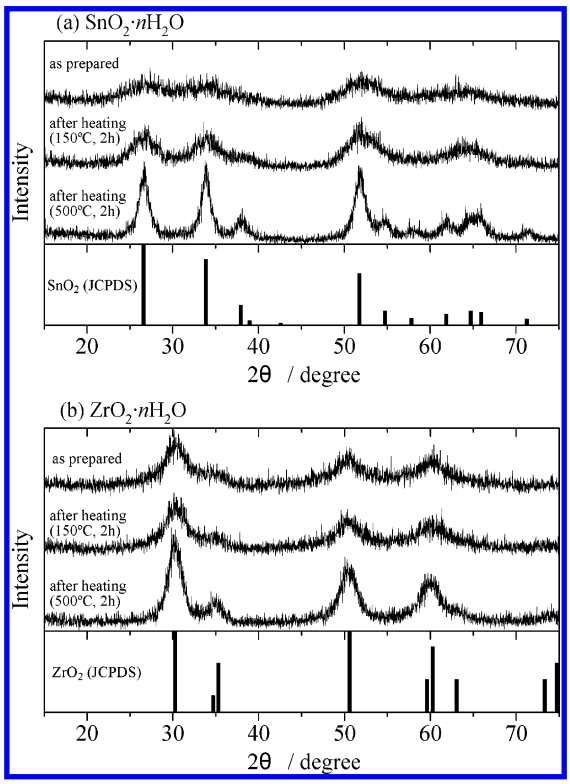

Figure 5. XRD profiles of (a) $SnO_2 \cdot nH_2O$ and (b) $ZrO_2 \cdot nH_2O$ after heating at 150 and 500 °C.

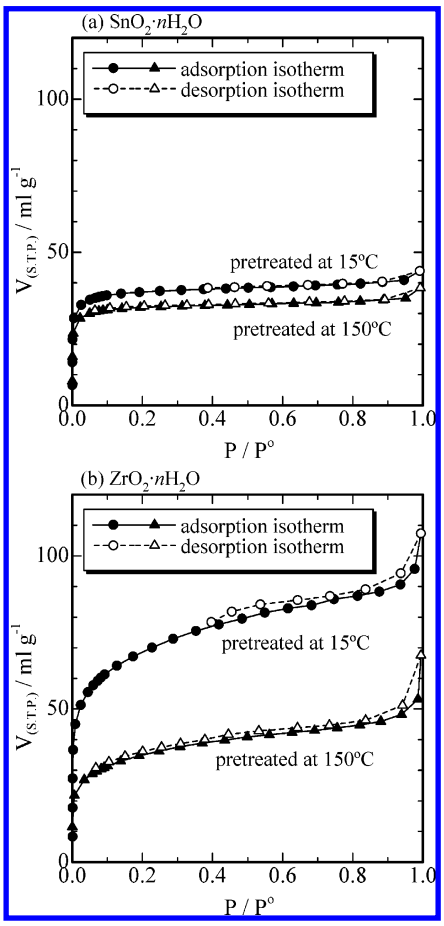

Figure 6. Nitrogen adsorption and desorption isotherms at 77 K for samples pretreated at 15 and 150 °C in vacuo: (a) $SnO_2 \cdot nH_2O$ and (b) $ZrO_2 \cdot nH_2O$.

respectively. The pretreatment was conducted in vacuo at 15 and 150 °C. On both hydrates, but particularly $SnO_2 \cdot nH_2O$, a rapid increase in volume of adsorbed nitrogen at a low relative pressure was observed. Hence it is concluded that the structure of these hydrates is similar to that of microporous materials, e.g., silica gel or carbon.[31,35,36] Even after pretreatment at 150 °C, the isotherm for $SnO_2 \cdot nH_2O$ was almost unchanged. Meanwhile, that for $ZrO_2 \cdot nH_2O$ shifted downward to a great extent. Estimated surface areas were 130−180 $m^2\ g^{-1}$ and 250−300 $m^2\ g^{-1}$ for $SnO_2 \cdot nH_2O$ and $ZrO_2 \cdot nH_2O$, respectively.

Parts a and b of Figure 7 show pore volume distributions of $SnO_2 \cdot nH_2O$ and $ZrO_2 \cdot nH_2O$, respectively. The MP method was applied to calculate the volume of micropores (<1 nm), and the DH method was used for the calculation of the volume of mesopores and macropores (>1 nm). Samples were pretreated in vacuo over 24 h at 15 and 150 °C. These figures indicate that micropores make up the pore volume of these hydrates. It is also clear that the average pore size in $SnO_2 \cdot nH_2O$ is smaller than that in $ZrO_2 \cdot nH_2O$.

TEM images of both hydrates are shown in Figure 8. $SnO_2 \cdot nH_2O$ comprises fine particles and shows a lattice fringe that corresponds to SnO_2, whereas $ZrO_2 \cdot nH_2O$ is observed to be amorphous. Furthermore, $SnO_2 \cdot nH_2O$ has a more rugged surface (grooves) than $ZrO_2 \cdot nH_2O$. These grooves will act as open micropores reserving water molecules and contribute to supply protons. It is presumed that the protons transport through 3-dimensional network constructed by connected particle surface.

In this way, it was confirmed that both hydrates are microporous materials, with the average pore size in $SnO_2 \cdot nH_2O$ being smaller than that in $ZrO_2 \cdot nH_2O$.

Relationship between the Conductivity and the Amount of Hydrated Water. Weight changes (TG curve) and differential weight changes (DTG curve) in dry air before and after

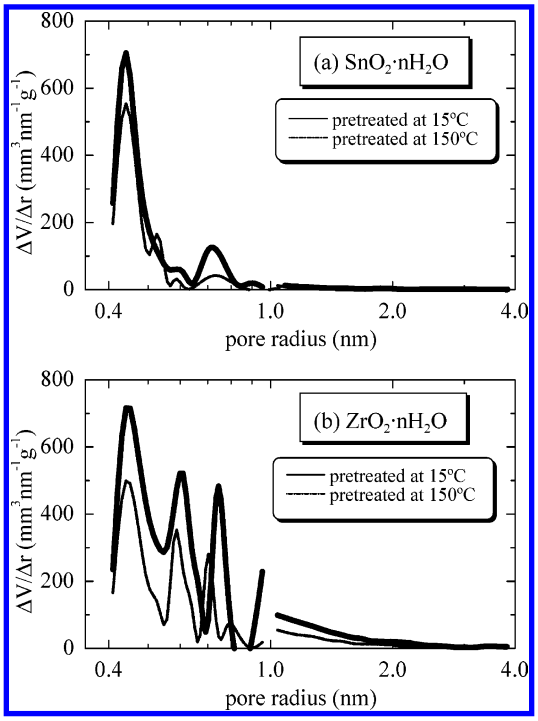

Figure 7. Pore volume distribution of (a) $SnO_2 \cdot nH_2O$ and (b) $ZrO_2 \cdot nH_2O$ calculated by the MP method (<1 nm) and DH method (>1 nm). Pretreatment of samples was conducted in vacuo over 24 h at 15 and 150 °C.

drying (at 150 °C, RH = 20%) for $SnO_2 \cdot nH_2O$ and $ZrO_2 \cdot nH_2O$ are shown in Figure 9a,b, respectively. $ZrO_2 \cdot nH_2O$ before drying showed a one-step decrease in weight, whereas $SnO_2 \cdot nH_2O$ before drying exhibited a two-step decrease that was confirmed by a high sharp peak at 25−130 °C and a low broad peak at 150−350 °C on the DTG curve. Compared with $ZrO_2 \cdot nH_2O$ after drying, $SnO_2 \cdot nH_2O$ after drying retained much water that was not eliminated at 150 °C.

Unlike nitrogen, which mainly physisorbs on a substance, water is adsorbed via hydrogen bonding so that the adsorption behavior of water may differ from that of nitrogen. The water-adsorption isotherms of hydrates at 150 °C were measured by pressure-resistive TG, and the results are shown in Figure 10. A rapid increase in the amount of hydrated water was also observed at low RH in the water-adsorption isotherm, similar to the nitrogen-adsorption isotherm of $SnO_2 \cdot nH_2O$. As expected from pore distribution data, the RH dependence of the amount of hydrated water in $SnO_2 \cdot nH_2O$ was weaker than that in $ZrO_2 \cdot nH_2O$.

It has been reported that hydrated water in $SnO_2 \cdot nH_2O$ can be classified into three types; structural water, bonded water, and adsorbed water, in order of decreasing bonding strength.[23] Structural water refers to condensed hydroxyl groups and is released at temperatures above 400 °C. Bonded water refers to the hydrogen-bonded water and is released gradually from 200 to 400 °C. Adsorbed water is defined as the water physisorbed to the bonded water and is released below 200 °C. These definitions are based on the manner of bonding. However, the adsorption energy depends also on the size of pores in which water molecules are adsorbed; that is, a smaller micropore has a higher adsorption energy. Judging from the microstructure of very small micropores in $SnO_2 \cdot nH_2O$, as shown in Figure 7a, the following classification seems to be reasonable: structural water, adsorbed water inside micropores, and adsorbed water outside micropores, in order of decreasing bonding strength. The two-step decreases in weight of $SnO_2 \cdot nH_2O$, as shown in Figure 9a, is attributable to the presence of small micropores. The structural water (hydroxyl groups) and the adsorbed water inside micropores in $SnO_2 \cdot nH_2O$ are difficult to be released at high temperatures and low humidities. This will result in the weak humidity dependence and dry resistance of proton conductivity

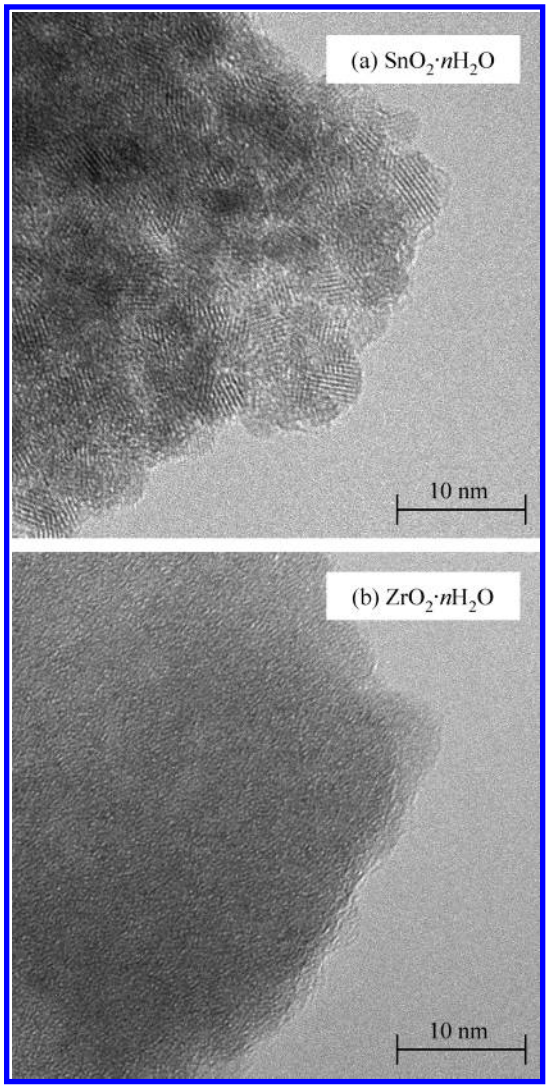

Figure 8. TEM images of (a) $SnO_2 \cdot nH_2O$ and (b) $ZrO_2 \cdot nH_2O$.

In Figure 7, the reduction of the pore volume of $SnO_2 \cdot nH_2O$ due to heating at 150 °C was slight (from 0.058 to 0.049 mL/g). On the other hand, the decrease in that of $ZrO_2 \cdot nH_2O$ was large (from 0.122 to 0.057 mL/g). Such a large decrease will cause the irreversible drop of conductivity for $ZrO_2 \cdot nH_2O$ after drying at 150 °C. As shown in Figure 10, gravimetric increases of 4.8 and 9.9 wt % were observed for $SnO_2 \cdot nH_2O$ and $ZrO_2 \cdot nH_2O$, respectively, after a change in RH from ~0 to 100% at 150 °C. If these increases are attributable to the occupation of pores by adsorbed water, gravimetric increases should be 4.9 and 5.7 wt %. The observed value agrees closely with the theoretical value for $SnO_2 \cdot nH_2O$; hence the water adsorbed in pores can be regarded as"hydrated water". A large amount of water is adsorbed on the surface of a $ZrO_2 \cdot nH_2O$ particle because of the larger pores; thus there is a difference between the total adsorbed water volume and total pore volume. This is because a large amount of water was adsorbed on the surface of $ZrO_2 \cdot nH_2O$, which has mesopores and large surface area.

Proton conductivity is governed by the concentration and mobility of protons, and hydrated water acts as a proton source

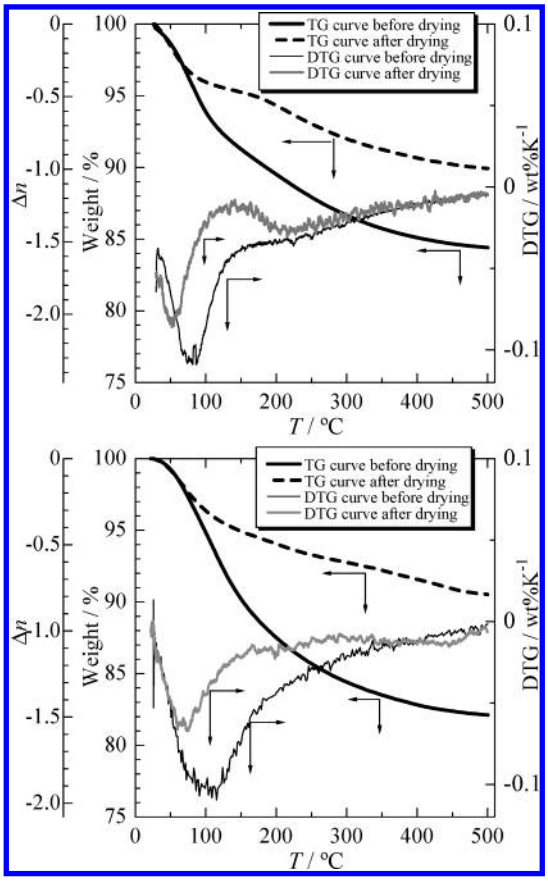

Figure 9. TG and DTG curves and Δn (variation of hydrated water) of (a) $SnO_2 \cdot nH_2O$ and (b) $ZrO_2 \cdot nH_2O$ in air before and after drying (150 °C, RH = 20%).

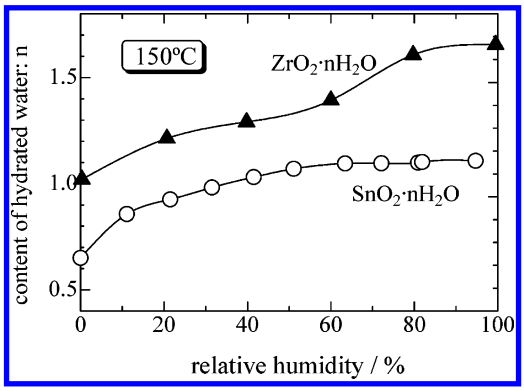

Figure 10. Relative humidity vs the content of hydrated water n in $SnO_2 \cdot nH_2O$ and $ZrO_2 \cdot nH_2O$ at 150 °C.

and a proton-conduction path. The relationship between the amount of hydrated water and the conductivity in the RH range ~0−100% is shown in Figure 11. The proton conductivity increased with an increase in the amount of hydrated water for each hydrate. Although the amount of hydrated water in $SnO_2 \cdot nH_2O$ is much smaller than that in $ZrO_2 \cdot nH_2O$, $SnO_2 \cdot nH_2O$ shows high conductivities and the changes of its conductivity and amount of hydrated water are in a narrow range compared with those of $ZrO_2 \cdot nH_2O$. This suggests that the concentration of mobile protons is not proportional to the amount of hydrated water. The hydrates have many hydroxyl groups, as mentioned before. The bond between Sn and O in hydroxyl groups has a covalent bond character because the electronegativity of Sn is higher than that of Zr. The O−H bond strength is then weakened, and dissociation of H^+ is enhanced. Dissociation of H^+ from water molecules hydrogen-bonded with hydroxyl

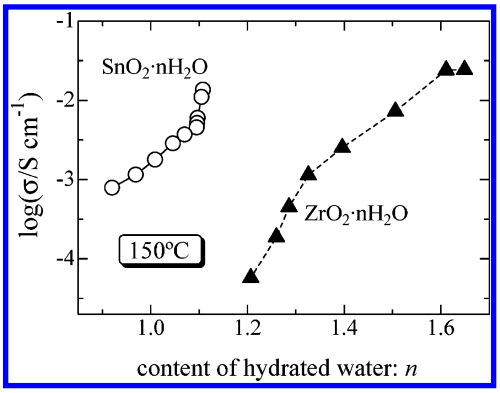

Figure 11. Content of hydrated water n vs conductivity of $SnO_2 \cdot nH_2O$ and $ZrO_2 \cdot nH_2O$ at 150 °C.

groups will also be enhanced in the same manner. Actually, it has been reported that an acid ionization constant (pK_a) for aqueous Sn^{4+} is smaller than that for aqueous Zr^{4+};[37] hence, it is presumed that partial negative charge on oxygen of SnO_2 is smaller than that of ZrO_2 and SnO_2 easily releases protons on surface. In this way, from the high electronegativity of Sn, it is assumed that $SnO_2 \cdot nH_2O$ shows high proton conductivity equivalent to that of $ZrO_2 \cdot nH_2O$ at high RH even though the amount of hydrated water is less than that of $ZrO_2 \cdot nH_2O$.

For many proton-conductive materials, a high proton conductivity is achieved by adding sulfuric acid or phosphoric acid to the material. In this study, however, high proton conductivity was achieved as a result of the acidity and micropore structure of the $SnO_2 \cdot nH_2O$ surface, without the addition of other acids. The combined effect of the control of microstructure and the doping of acids may lead to further improvement of proton conductivity.

Conclusions

Nitrogen adsorption analyses indicated the presence of a large amount of micropores with pore radius below 1 nm in $SnO_2 \cdot nH_2O$ and $ZrO_2 \cdot nH_2O$, but the average pore size of $SnO_2 \cdot nH_2O$ was smaller than that of $ZrO_2 \cdot nH_2O$. The unevenness of the $SnO_2 \cdot nH_2O$ surface suggested the presence of micropores. The amounts of hydrated water n were 0.7−1.2 for $SnO_2 \cdot nH_2O$ and 1.0−1.7 for $ZrO_2 \cdot nH_2O$ under relative humidities (RH) of ~0−95% at 150 °C. The hydrated water can be regarded as the water adsorbed in micropores in $SnO_2 \cdot nH_2O$. A proton conductivity of about 10^{-2} S cm^{-1} was observed at 95% RH and 150 °C for both hydrates. The conductivity decreased with decreasing RH, but $SnO_2 \cdot nH_2O$ maintained a higher conductivity than that of $ZrO_2 \cdot nH_2O$ under low RH. Although $SnO_2 \cdot nH_2O$ has a smaller amount of hydrated water than $ZrO_2 \cdot nH_2O$, $SnO_2 \cdot nH_2O$ showed a conductivity as high as that of $ZrO_2 \cdot nH_2O$. The high conductivity was assumed to be due to the high electronegativity of Sn and resulting high concentration of dissociated protons. $SnO_2 \cdot nH_2O$ maintained adsorbed water tightly, even at low humidity, because of the high adsorption energy of small micropores. This was considered to result in the weak dependence of conductivity on RH for $SnO_2 \cdot nH_2O$.

Acknowledgment. We thank Mr. T. Tsuru, Institute of Industrial Science (the University of Tokyo), for nitrogen adsorption measurements and Dr. Y. Inoue, Nissan Arc Ltd., for TEM observation.

References and Notes

(1) England, W. A.; Cross, M. G.; Hamnett, A.; Wiseman, P. J.; Goodenough, J. B. *Solid State Ionics* **1980**, *1*, 231−249.

(2) Barboux, P.; Morineau, R.; Livage J. *Solid State Ionics* **1988**, *27*, 221−225.
(3) Barrado, J. R. R.; Criado, C.; Lopez, A. J.; Pastor, P. O.; Castellon, E. R. *Solid State Ionics* **1991**, *46*, 73−76.
(4) Kreuer, K.-D. *Chem. Mater.* **1996**, *8*, 610−641.
(5) Norby, T. *Solid State Ionics* **1999**, *125*, 1−11.
(6) Alberti, G.; Casciola, M.; Cavalaglio, S.; Vivani, R. *Solid State Ionics* **1999**, *125*, 91−97.
(7) Takahashi, T. *Nenryou-Denchi*, 2nd ed.; Kyouritsu Syuppan: Tokyo, 1984.
(8) Laminie, J.; Dicks A. *Fuel Cell System Explained*; Wiley: England, 2000.
(9) Vaivars, G.; Azens, A.; Granqvist, C. G. *Solid State Ionics* **1999**, *119*, 269−273.
(10) Nogami M.; Nagao R.; Wong C.; Kasuga T.; Hayakawa T. *J. Phys. Chem. B* **1999**, *103*, 9468−9472.
(11) Hinokuma, K.; Ata, M. *Chem. Phys. Lett.* **2001**, *341*, 442−446.
(12) Matsuda, A.; Kanzaki, T.; Tadanaga, K.; Tatsumisago M.; Minami, T. *Electrochim. Acta* **2002**, *47*, 939−944.
(13) Costamagna, P.; Yang, C.; Bocarsly A. B.; Srinivasan, S. *Electrochim. Acta* **2002**, *47*, 1023−1033.
(14) Matsuda, A.; Kanzaki, T.; Tadanaga, K.; Tatsumisago M.; Minami, T. *Solid State Ionics* **2002**, *154*−*155*, 687−692.
(15) Schechter, A.; Savinell, R. F. *Solid State Ionics* **2002**, *147*, 181−187.
(16) England, W. A.; Cross, M. G.; Hamnett, A.; Wiseman, P. J.; Goodenough, J. B. *Solid State Ionics* **1980**, *1*, 231−249.
(17) Giesekke, E. W.; Gutowsky, H. S.; Kirkov, P.; Laitenen, H. A. *Inorg. Chem.* **1967**, *6*, 1294−1297.
(18) Kaneko, S.; Kanamori, J.; Imoto, F. *Nihon Kagaku Kaishi* **1976**, *6*, 906−910.
(19) Dobrovolsky, Y.; Leonova, L.; Nadkhina, S.; Panina, N. *Solid State Ionics* **1999**, *119*, 275−279.
(20) Miura, N.; Ozawa, Y.; Yamazoe, N. *Nihon Kagaku Kaishi* **1988**, *12*, 1954−1960.
(21) Clearfield, A. *Inorg. Chem.* **1964**, *3*, 146−148.
(22) Livage, J.; Doi, K.; Mazieres, C. *J. Am. Ceram. Soc.* **1968**, *51* (6), 349−353.
(23) Murase, Y.; Katou, E. *Yogyo Kyoukaishi* **1976**, *84* (10), 478−481.
(24) Matsui, K.; Suzuki, H.; Ohgai, M. *J. Am. Ceram. Soc.* **1995**, *78* (1), 146−152.
(25) Matsui, K.; Ohgai, M. *J. Am. Ceram. Soc.* **1997**, *80* (8), 1949−1956.
(26) C-.Hu, M. Z.; Harris, M. T.; Byers, C. H. *J. Colloid and Interface Sci.* **1998**, *198*, 87−99.
(27) Matsui, K.; Ohgai, M. *J. Am. Ceram. Soc.* **2000**, *83* (6), 1386-1392.
(28) Matsui, K.; Ohgai, M. *J. Am. Ceram. Soc.* **2000**, *85* (3), 545−553.
(29) Hara, S.; Miyayama, M.; Kudo, T. *Trans. Mater. Res. Soc. Jpn.* **2001**, *26* (3), 1071−1074.
(30) Hara, S.; Sakamoto, H.; Miyayama, M.; Kudo, T. *Solid State Ionics* **2002**, *154*−*155*, 679−685.
(31) Mikhail, R. S.; Brunauer, S.; Bodor, E. E. *J. Colloid Interface Sci.* **1968**, *26*, 45−53.
(32) Lippens, B. C.; de Boer, J. H. *J. Catal.* **1965**, *4*, 319−323.
(33) Dollimore, D.; Heal, G. R. *J. Appl. Chem.* **1964**, *14*, 109−114.
(34) Colomban, P. *PROTON CONDUCTORS*−*Solids, membranes and gels-materials and devices*; Cambridge University Press: Cambridge, U.K., 1992; Chapter 3.
(35) Alverti, G.; Costantino, U.; Marmottini, F.; Vivani, R.; Zappelli, P. *Microporous Mesoporous Mater.* **1998**, *21*, 297−304.
(36) Stoeckli, F.; Guillot, A.; Slasli, A. M.; Hugi-Cleary, D. *Carbon* **2002**, *40*, 383−388.
(37) Tanaka, K.; Ozaki, A. *J. Catal.* **1967**, *8*, 1−7.